**PSFC/JA-06-20**

# Short wavelength effect on the collisionless neoclassical polarization and residual zonal flow level

Yong Xiao and Peter J. Catto

MIT Plasma Science and Fusion Center, 167 Albany Street,
Cambridge, MA 02139, U.S.A.

This work was supported by the U.S. Department of Energy, Grant No. DE-FG02-91ER-54109.

*Submitted for publication in the Physics of Plasma (August 2006)*

# Short wavelength effects on the collisionless neoclassical polarization and residual zonal flow level

Yong Xiao and Peter J. Catto

*MIT Plasma Science and Fusion Center, Cambridge, MA 02139, U.S.A.*

(Dated: 7/27/2006)

## Abstract

Sheared zonal flow helps to reduce the turbulent transport caused by the ion temperature gradient (ITG) mode. Rosenbluth and Hinton (R-H) calculated the residual zonal flow level for radial wavelengths that are much larger than the ion poloidal gyroradius. Their calculation is extended to treat arbitrary radial wavelengths. For the radial wavelengths that approach the ion poloidal gyroradius, but are much larger than the ion gyroradius, an analytical formula is obtained. For radial wavelengths that are comparable or shorter than the poloidal ion gyroradius and the ion gyroradius a numerical solution is provided. These small radial wavelength results are then extended into the electron temperature gradient (ETG) regime, where the residual zonal flow level is large but ineffective in regulating the turbulence, indicating that the conventional R-H explanation that zonal flow regulates turbulence is incomplete.

## I. INTRODUCTION

Radial heat transport in tokamaks is believed to be largely due to plasma turbulence caused by microinstabilities. The turbulence generates a sheared zonal flow having a radially varying axisymmetric electrostatic potential with no poloidal variation, that can act to regulate these transport losses [1]. Three of the most important instabilities are the ion temperature gradient (ITG) mode [2], the trapped electron mode (TEM) [3], and electron temperature gradient (ETG) mode [4]. It is known that sheared zonal flow reduces the saturated amplitude of ITG modes [5][6], especially near marginality where a nonlinear upshift in the stability threshold results [3][7]. Recent nonlinear gyrokinetic simulations of TEM turbulence have revealed a nonlinear upshift in the critical density gradient due to zonal flows [8]. Moreover, ETG and ITG instabilities are known to be closely related (they are referred to as being isomorphic to lowest order), but with differing (non-isomorphic) zonal flows possibly due to different parasitic instabilities [9]. Indeed, for a fixed initial potential perturbation, the residual zonal flow level is much larger for ETG wavelengths than for ITG wavelengths since the polarization of the electrons as well as the ions must be retained [9]. For the ETG case where the radial wavelength is smaller than the ion gyroradius, the ion response becomes closely adiabatic and the electron polarization is important.

Clearly, the residual zonal flow level is an important ingredient of the turbulence level in a tokamak [10][11], but other effects must come into play to explain the difference between turbulent ITG and ETG behavior. In the following sections, we extend the collisionless zonal flow work of Rosenbluth and Hinton to arbitrary radial wavelengths for the ITG and ETG modes. We only consider the collisionless limit and verify that the behavior of the residual is the same as observed by Jenko *et al.* [9].

The zonal flow in codes is observed to have much less of an impact on ETG turbulence than on ITG turbulence, presumably because parasitic or secondary instabilities are unable to generate an appreciable zonal flow [9]. Kim, Holland and Diamond [12] attribute some of this difference to the fact that this short wavelength poloidal zonal flow is collisionally damped, while Candy and Waltz [13] have found that the non-adiabatic behavior of the ions is important to retain. Both of these explanations hint that there are differences between ITGs and ETGs that can result differing secondary effects which may well be playing the key role in generating different zonal flows.

In the original Rosenbluth-Hinton ($R$-$H$) zonal flow model [10], turbulent fluctuations build a charge source within a time much smaller than the bounce time, but much larger than the gyroperiod. Thus, an initial zonal flow potential is produced by this turbulence charge source through classical polarization $\varepsilon_{k,cl}^{pol}$ that is due to particle departure from the guiding center. This process happens on a time scale of several ion gyration periods. After several bounce times, the initial potential is modified by the total polarization $\varepsilon_{k}^{pol}$, which includes not only classical polarization, but also the neoclassical polarization $\varepsilon_{k,nc}^{pol}$ that is due to the guiding center departure from the flux surface. When the radial wavelength is much larger than the ion gyroradius, the two contributions are completely decoupled and the total can be written as a sum of the classical and neoclassical polarizations $\varepsilon_{k}^{pol} = \varepsilon_{k,cl}^{pol} + \varepsilon_{k,nc}^{pol}$. The long time behavior of zonal flow is then determined by the zero frequency response of the neoclassical polarization, and the so called residual zonal flow level is given by

$$\frac{\phi_k\left(t=\infty\right)}{\phi_k\left(t=0\right)} = \frac{\varepsilon_{k,cl}^{pol}}{\varepsilon_{k,cl}^{pol} + \varepsilon_{k,nc}^{pol}\left(0\right)}, \tag{1}$$

This R-H zonal flow model has been verified for the weak turbulence case by many numerical codes [2][9][7][14]. The original $R$-$H$ collisionless calculation requires radial wavelength to be much larger than the poloidal ion gyroradius. However, recent advances in experiments [15] and simulations [16] suggest that radial wavelengths in the range of several ion poloidal gyroradius may play an important role. Hence, it is meaningful to extend the original R-H calculation to include these shorter wavelengths. Moreover, fluctuations associated with ETG turbulence are comparable to the electron gyroradius. The zonal flow response due to ETG turbulence can be evaluated by essentially the same technique. Indeed, Jenko *et al.* [9] have already numerically evaluated the residual to find behavior similar to what we will find here by an independent semi-analytical method.

In section II, we use the drift kinetic equation to calculate the collisionless neoclassical polarization for radial wavelengths that are larger than one ion gyroradius by generalizing the Hinton-Rosenbluth procedure [11] of evaluating the distribution function and polarization. In section III, we evaluate the neoclassical polarization and associated residual zonal flow for somewhat shorter wavelengths, by distinct analytical and numerical approaches. In section IV, we evaluate the residual zonal flow for arbitrary wavelengths that are allowed to be much shorter than the ion gyroradius, but still much larger than electron poloidal gyroradius. In section V, we proceed to consider even shorter wavelengths, from comparable to the electron

poloidal gyroradius to even smaller than the electron gyroradius.

## II. NEOCLASSICAL POLARIZATION FOR LARGE WAVELENGTHS

When the radial electric field of a tokamak changes with time, it leads to a polarization current due to local orbit departures from magnetic field lines. The polarization of the media $\varepsilon^{pol}$ can be defined by the linear response $\varepsilon^{pol}\partial\mathbf{E}/\partial t = 4\pi\mathbf{J}^{pol}$, or in *Fourier* space by $-i\mathbf{k}_\perp\varepsilon_k^{pol}\partial\phi_k/\partial t = 4\pi\mathbf{J}_k^{pol}$. The polarization current $\mathbf{J}_k^{pol}$ itself must satisfy the continuity equation on a flux surface, $\partial\left\langle\rho_k^{pol}(t)\right\rangle/\partial t + \left\langle i\mathbf{k}_\perp\cdot\mathbf{J}_k^{pol}(t)\right\rangle = 0$, where $\langle\rangle$ is the flux surface average and $\rho_k^{pol}$ the polarization charge density. Therefore, in the Fourier and frequency domain, the polarization can be defined by

$$\varepsilon_{k,nc}^{pol}(p)\left\langle k_\perp^2\right\rangle\phi_k(p) \equiv -4\pi\sum Ze\left\langle\int d^3v f_k(p)\right\rangle, \tag{2}$$

where $p = i\omega$ is the frequency variable, and $f_k$ is the perturbed species distribution. Since ion polarization is much larger than electron polarization, only the ion contribution needs to be considered in the polarization calculation for ITG modes [10][11]. Later, when considering ETG modes, we will include the electron polarization.

When the radial wavelength is still much larger than the ion gyroradius, as in most ITG experiments and simulations, the neoclassical polarization can be separated from the total plasma polarization. To calculate the neoclassical polarization, we focus on the gyrophase independent part of the ion distribution, which we still denote as $f_k$ for convenience. This gyrophase independent distribution $f_k$ is driven by the axisymmetric zonal flow potential $\phi_k$ [11]:

$$\frac{\partial f_k}{\partial t} + \left(v_{\shortparallel}\mathbf{b}\cdot\nabla + i\omega_D\right)f_k - C_{ii}\left\{f_k\right\} = -\frac{e}{T_i}F_0\left(v_{\shortparallel}\mathbf{b}\cdot\nabla + i\omega_D\right)\phi_k, \tag{3}$$

where $F_0$ is a local *Maxwellian*, and the magnetic drift frequency is $\omega_D = \mathbf{k}_\perp\cdot\mathbf{v}_d$. Here we assume all perturbed quantities take a eikonal form, $\phi(\mathbf{r},t) = \sum_k \phi_k e^{iS}$ with the eikonal $S = S(\psi)$ and the radial wave vector $\mathbf{k}_\perp = \nabla S$. The magnetic drift $\mathbf{v}_d = \frac{\mathbf{b}}{\Omega}\times\left(\mu\nabla B + v_\parallel^2\mathbf{b}\cdot\nabla\mathbf{b}\right)$ has the usual radial component form $\mathbf{v}_d\cdot\nabla\psi = v_{\shortparallel}\mathbf{b}\cdot\nabla\left(\frac{Iv_{\shortparallel}}{\Omega}\right)$. Following *H-R* it is convenient to define $\omega_D = v_{\shortparallel}\mathbf{b}\cdot\nabla Q$ with $Q = IS'v_{\shortparallel}/\Omega$. Notice $Q \sim k_\perp\rho_p$, where $\rho_p = \rho_i q/\varepsilon$ is the poloidal gyroradius. The independent velocity variables used in the preceding equation are kinetic energy $E = v^2/2$ and magnetic moment $\mu = v_\perp^2/2B$. Here we will only consider the collisionless large aspect ratio circular flux surface limit as in *R-H*.

Since the zonal flow potential is independent of position along a field line, the preceding drift kinetic equation in the collisionless limit can be further simplified to

$$\frac{\partial f_k}{\partial t} + \left(v_{\shortparallel}\mathbf{b}\cdot\nabla + iv_{\shortparallel}\mathbf{b}\cdot\nabla Q\right) f_k = -\frac{e\phi_k}{T_i}F_0 iv_{\shortparallel}\mathbf{b}\cdot\nabla Q. \tag{4}$$

To solve this equation, we follow *H-R* [11] by defining

$$f_k \equiv -\frac{e}{T_i}\phi_k F_0 + H_k e^{-iQ}. \tag{5}$$

Then, the new distribution to be determined, $H_k$, satisfies the following equation,

$$\frac{\partial H_k}{\partial t} + v_{\shortparallel}\mathbf{b}\cdot\nabla H_k = e^{iQ}\frac{e}{T_i}F_0\frac{\partial \phi_k}{\partial t}. \tag{6}$$

This equation can be solved perturbatively by expanding in $\omega/\omega_t \ll 1$ [10], $H_k = H_k^{(1)} + H_k^{(2)} + ...$, where $\omega_t$ is the transit frequency. The leading order equation is simply $v_{\shortparallel}\mathbf{b}\cdot\nabla H_k^{(1)} = 0$, giving $H_k^{(1)}$ independent of poloidal angle $\theta$, i.e., $H_k^{(1)} = H_k^{(1)}(E,\lambda)$, where the pitch angle $\lambda \equiv \mu B_0/E$ with $B_0$ the on axis value of the magnetic field. A transit average of the next order equation gives

$$\frac{\partial H_k^{(1)}}{\partial t} = \overline{e^{iQ}}\frac{e}{T_i}F_0\frac{\partial \phi_k}{\partial t}, \tag{7}$$

where the bounce average is defined as $\overline{A} = \oint \frac{dl}{v_\parallel} A / \oint \frac{dl}{v_\parallel}$, with $\oint$ denoting integration around a full trapped particle bounce period or a complete passing particle poloidal transit time. The preceding equation can easily be integrated to obtain $H_k^{(1)} = \overline{e^{iQ}}\frac{e\phi_k}{T_i}F_0$. Ignoring higher order terms in the $\omega/\omega_t$ expansion, the perturbed distribution $f_k$ becomes

$$f_k \cong \frac{e}{T_i}\phi_k F_0\left(e^{-iQ}\overline{e^{iQ}} - 1\right). \tag{8}$$

Therefore, the ion neoclassical polarization defined in Eq.(2) becomes

$$\varepsilon_{k,nc}^{pol} = \frac{\omega_{pi}^2/\omega_{ci}^2}{\langle k_\perp^2\rangle \rho_i^2}\left(1 - \frac{1}{n_0}\left\langle \int d^3v F_0 e^{-iQ}\overline{e^{iQ}}\right\rangle\right), \tag{9}$$

where $\omega_{pi} = \sqrt{4\pi e^2 n_0/m_i}$ is the ion plasma frequency, $\omega_{ci} = eB_0/m_i c$ is the ion gyrofrequency at the magnetic axis, $\rho_i = v_i/\omega_{ci}$ is the ion gyroradius, and $v_i = \sqrt{T_i/m_i}$ is the ion thermal speed.

In the large wavelength limit considered by R-H, $Q \ll 1$, so that adiabatic ion response is nearly canceled, and the preceding equation reduces to

$$\begin{aligned}\varepsilon_{k,nc}^{pol} &= \frac{\omega_{pi}^2/\omega_{ci}^2}{\langle k_\perp^2\rangle \rho_i^2}\frac{1}{n_0}\left\langle \int d^3v F_0\left(\overline{Q^2} - \overline{Q}^2\right)\right\rangle \\ &\to \frac{\omega_{pi}^2}{\omega_{ci}^2}\frac{q^2}{\varepsilon^2}1.6\varepsilon^{3/2},\end{aligned} \tag{10}$$

where a simple large aspect ratio, circular tokamak model ($dl = qR_0 d\theta$ with $R_0$ the major radius of the magnetic axis), is assumed to obtain the final form of this equation. According to Eq.(1), after employing $\varepsilon_{k,cl}^{pol} = \omega_{pi}^2/\omega_{ci}^2$ for those long wavelengths satisfying $k_\perp^2 \rho_i^2 \ll 1$, the associated residual zonal flow becomes

$$\frac{\phi_k\left(t=\infty\right)}{\phi_k\left(t=0\right)} = \frac{1}{1+\frac{q^2}{\varepsilon^2}1.6\varepsilon^{3/2}}, \tag{11}$$

which is the celebrated *R-H* collisionless residual zonal flow level.

## III. WAVELENGTHS CLOSE TO A POLOIDAL GYRORADIUS

It is not possible to integrate Eq.(9) analytically for arbitrary $Q$. Instead, we first extend the $Q$ expansion to $Q^4$ analytically, making the result valid for $Q$ close to unity. Then we calculate the neoclassical polarization for arbitrary $Q$ numerically. A comparison between the analytical and numerical result is shown in the final part of this section. The following calculations employ the large aspect ratio, circular flux surface model as in *R-H*.

### A. Analytical Calculation

To evaluate integrals analytically, we employ the volume element $d^3v = 4\pi BEdEd\lambda/\left(B_0\left|v_{\shortparallel}\right|\right)$, where $\lambda \equiv \mu B_0/E$ is the pitch angle variable and $B_0$ is the magnetic field at the magnetic axis. Equation (9) can be expanded to order $Q^4$ to obtain the following approximate analytical result for the neoclassical polarization:

$$\varepsilon_{k,nc}^{pol} \cong -\frac{\omega_{pi}^2/\omega_{ci}^2}{k_\perp^2\rho_i^2}\frac{1}{2\pi^{3/2}}\int_0^{+\infty} dy e^{-y}\sqrt{y}\frac{2\pi}{\oint d\theta h}\int d\lambda \oint \frac{d\theta}{\xi}$$
$$\left(\overline{Q}^2 - \overline{Q^2} + \frac{1}{12}\overline{Q^4} + \frac{1}{4}\overline{Q^2}^2 - \frac{1}{3}\overline{Q}\ \overline{Q^3}\right), \tag{12}$$

where $y = m_i E/T_i$ and $Q = IS'\xi h/\Omega_0$, with $\xi = \left|v_\parallel\right|/v$, and $h = R/R_0 = B_0/B = 1+\varepsilon\cos\theta$ based on a simple concentric circle tokamak model. This equation is evaluated for $\varepsilon \ll 1$, accurate to $\mathcal{O}\left(\varepsilon^{7/2}\right)$, in the Appendix to find

$$\varepsilon_{k,nc}^{pol} = \frac{\omega_{pi}^2}{\omega_{ci}^2}\frac{q^2}{\varepsilon^2}\Theta \tag{13}$$

with the factor $\Theta$ defined as

$$\Theta = (1.6\varepsilon^{3/2} + \frac{1}{2}\varepsilon^2 + 0.36\varepsilon^{5/2}) - 2.44\varepsilon^{5/2}k_\perp^2\rho_p^2, \tag{14}$$

and where $k_\perp\rho_p$ is defined as

$$k_\perp\rho_p = \frac{IS'}{\Omega_0}\sqrt{\frac{T_i}{m_i}} = k_\perp\rho_i\frac{q}{\varepsilon}. \tag{15}$$

As a result, the collisionless residual zonal flow level $\gamma$ for finite poloidal gyroradius and finite inverse aspect ratio becomes

$$\gamma \equiv \frac{\phi_k\left(t=\infty\right)}{\phi_k\left(t=0\right)} = \frac{1}{1+q^2\Theta/\varepsilon^2}. \tag{16}$$

This analytic expression allows $k_\perp\rho_p$ to be closer to one, but still requires $k_\perp^4\rho_p^4$ to be much smaller than one. It also provides a benchmark to check the $Q\sim 1$ numerical calculation of $\varepsilon_k^{pol}$ considered next.

### B. Numerical Calculation

A numerical calculation is necessary when $k_\perp^4\rho_p^4$ is no longer small. First, we notice

$$\oint \frac{d\theta}{\xi}e^{-iQ}\overline{e^{iQ}} = \left(\oint\frac{d\theta}{\xi}\right)^{-1}\left[\left(\oint\frac{d\theta}{\xi}\cos Q\right)^2 + \left(\oint\frac{d\theta}{\xi}\sin Q\right)^2\right]. \tag{17}$$

However, this form is not very convenient for numerical integration because the function $\cos Q$ contains the unity factor that must cancel in Eq.(9), leaving very small variations, of $\mathcal{O}\left(\varepsilon^{3/2}\right)$ for the large radial wavelength case. Hence, it is useful to transform the preceding equation to the following form,

$$\oint \frac{d\theta}{\xi}e^{-iQ}\overline{e^{iQ}} = \oint\frac{d\theta}{\xi} + K\left(Q\right), \tag{18}$$

with the function $K\left(Q\right)$ defined as

$$K\left(Q\right) = 2\oint\frac{d\theta}{\xi}\left(\cos Q - 1\right) + \left(\oint\frac{d\theta}{\xi}\right)^{-1} \left\{\left[\oint\frac{d\theta}{\xi}\left(\cos Q-1\right)\right]^2 + \left(\oint\frac{d\theta}{\xi}\sin Q\right)^2\right\}. \tag{19}$$

As a result, the polarization becomes

$$\varepsilon_{k,nc}^{pol} = -\frac{\omega_{pi}^2/\omega_{ci}^2}{k_\perp^2\rho_i^2}\frac{1}{2\pi^{3/2}}\int_0^{+\infty} dy e^{-y}\sqrt{y}\int d\lambda K\left(Q\right). \tag{20}$$

Next, we carry out the integration in Eq.(20), noting that the $\sin Q$ integration in Eq.(19) vanishes for trapped particles due to the odd parity of the integrand. The transit average of an arbitrary function $F\left(\theta,\lambda,y\right)$ can be evaluated using

$$\oint\frac{d\theta}{\xi}F\left(\theta,\lambda,y\right) = \left\{\begin{array}{c} 2\int_0^{\pi} d\theta\sqrt{\frac{1+\varepsilon\cos\theta}{1+\varepsilon\cos\theta-\lambda}}F\left(\theta,\lambda,y\right), \text{ for } \lambda<1-\varepsilon \\ 2\int_0^{\theta_b} d\theta\sqrt{\frac{1+\varepsilon\cos\theta}{1+\varepsilon\cos\theta-\lambda}}F\left(\theta,\lambda,y\right), \text{ for } 1-\varepsilon<\lambda<1+\varepsilon \end{array}\right\}, \tag{21}$$

with $\theta_b = \arccos\left[\left(\lambda-1\right)/\varepsilon\right]$ the turning point angle. The function $F\left(\theta,\lambda\right)$ is either 1, $\sin Q$ or $\cos Q-1$, for the different integrals in Eq.(19). For the energy integral, Gaussian quadrature is applied to make the integration accurate even for large $k_\perp\rho_p$.

### C. Comparison of Analytic and Numerical Results

We compare the neoclassical polarization computed by the preceding two approaches in Fig. VII. The analytic formula is good for wavelengths up to $k_\perp\rho_p\sim 0.7$, and inverse aspect ratio up to $\varepsilon = 0.3$.

We also plot the residual zonal flow level as a function of $k_\perp\rho_i$, as shown in Fig. VII for a wavenumber independent initial potential perturbation $\phi\left(t=0\right)$. When $k_\perp\rho_p \ll 1$, there is a plateau which corresponds to the *R-H* collisionless residual. As $k_\perp\rho_p$ approaches unity, the radial zonal flow level increases with the radial wavenumber $k_\perp$. Specifically according to Eq.(16), when $q^2k_\perp^2\rho_p^2\sqrt{\varepsilon}\sim 1$ or $k_\perp\rho_i\sim\varepsilon^{3/4}/q^2$, the zonal flow residual begins to grow with $k_\perp\rho_i$. Therefore, in Fig. VII we see that the curve of $\varepsilon = 0.2$ starts to grow earlier than that of $\varepsilon = 0.3$ as $k_\perp\rho_i$ increases.

## IV. RESIDUAL FOR WAVELENGTHS COMPARABLE TO THE ION GYRORADIUS

When the radial wavelengths becomes comparable to the ion gyroradius, the neoclassical and classical ion polarization no longer decouple and only a numerical solution is possible.

In this case we can easily extend our numerical calculation of the zonal flow residual to wavelengths comparable to $\rho_i$, but much larger than the electron poloidal gyroradius.

In the collisionless case, the gyrokinetic equation gives the following total polarization [10]

$$\varepsilon_k^{pol}(p) = \frac{\omega_{pi}^2/\omega_{ci}^2}{\langle k_\perp^2 \rangle \rho_i^2}\left(1 - \frac{1}{n_0}\left\langle \int d^3v F_0 J_0 e^{-iQ}\overline{J_0 e^{iQ}}\right\rangle\right). \tag{22}$$

Comparing this result to the collisionless neoclassical polarization in Eq. (9), we see that the preceding equation includes finite gyroradius effects through the *Bessel* function $J_0 = J_0\left(\frac{k_\perp v_\perp}{\omega_{ci}}\right)$. Therefore, the residual zonal flow level $\gamma$ is now given by

$$\gamma \equiv \frac{\phi_k(t=\infty)}{\phi_k(t=0)} = \frac{1 - \frac{1}{n_0}\left\langle \int d^3v F_0 J_0^2\right\rangle}{1 - \frac{1}{n_0}\left\langle \int d^3v F_0 J_0 e^{-iQ}\overline{J_0 e^{iQ}}\right\rangle}. \tag{23}$$

We first look at the residual zonal flow qualitatively. Use of a *Schwarz inequality* gives

$$\overline{J_0 e^{-iQ}}\ \overline{J_0 e^{iQ}} \leq \overline{J_0^2}. \tag{24}$$

Therefore,

$$\left\langle \int d^3v F_0 J_0 e^{-iQ}\overline{J_0 e^{iQ}}\right\rangle \leq \left\langle \int d^3v F_0 J_0^2\right\rangle. \tag{25}$$

We also have $J_0^2 \leq 1$. Hence, the residual factor

$$\frac{\phi_k(t=\infty)}{\phi_k(t=0)} \leq 1. \tag{26}$$

When the radial wavelength is large or $Q \ll 1$, the residual zonal flow level is reduced by neoclassical polarization. When the radial wavelength is extremely small or $k_\perp \rho_i \gg 1$, both classical polarization and neoclassical polarization are unable to reduce the zonal flow.

It is straight forward to generalize the numerical calculation for residual zonal flow based on Eq.(23). We need only change the factor $K(Q)$ in Eq. (19) to the following:

$$K(Q) = 2\oint \frac{d\theta}{\xi}(J_0 \cos Q - 1) + \left(\oint \frac{d\theta}{\xi}\right)^{-1} \left\{\left[\oint \frac{d\theta}{\xi}(J_0 \cos Q - 1)\right]^2 + \left(\oint \frac{d\theta}{\xi} J_0 \sin Q\right)^2\right\}. \tag{27}$$

The residual zonal flow then becomes

$$\gamma = \frac{\phi_k(t=\infty)}{\phi_k(t=0)} = \frac{1 - \langle \Gamma_0(b)\rangle}{-\frac{1}{2\pi^{3/2}}\int_0^{+\infty} dy e^{-y}\sqrt{y}\int d\lambda K(Q)}, \tag{28}$$

where the function $\Gamma_0(b) = I_0(b)\, e^{-b}$, with $I_0$ a modified *Bessel* function of the first kind and $b = k_\perp^2 \rho_i^2 B_0^2/B^2$.

We may then plot the zonal flow residual as a function of the perpendicular wave number $k_\perp \rho_i$, as shown in Fig. VII. When $k_\perp \rho_i < 0.1$, the small residual flow level is determined by the *R-H* polarization, which has no dependence on $k_\perp \rho_i$. When $0.1 < k_\perp \rho_i < 1$, there is transitional region where the residual zonal flow increases with $k_\perp \rho_i$. When $k_\perp \rho_i > 1$ the zonal flow is completely undamped. Notice that the $\varepsilon$ dependence of the residual $\gamma$ is rather weak for $\varepsilon \gtrsim 0.1$.

## V. RESIDUAL FOR ARBITRARY WAVELENGTHS

For ETG turbulence the radial wavelengths can be comparable to the electron gyroradius $\rho_e$. In such a short wavelength limit, the electron polarization effect can no longer be ignored. For a given initial charge density perturbation $e\delta n_k(t=0)$, the initial zonal flow potential is modified by the classical polarization from both ions and electrons,

$$\phi_k(t=0) = \frac{T_i \delta n_k(t=0)}{e\left[\tau\left(1 - \frac{1}{n_0}\left\langle \int d^3v F_0 J_0^2 \right\rangle\right) + 1 - \frac{1}{n_0}\left\langle \int d^3v F_{0e} J_{0e}^2 \right\rangle\right]}, \tag{29}$$

where $\tau = T_e/T_i$, the subscript $e$ is for electrons, and the ion subscript is not shown explicitly to maintain consistency with our previous notation. In the long time limit, the zonal flow potential is modified by the coupled classical and neoclassical polarization from both species,

$$\phi_k(t=\infty) = \frac{T_i \delta n_k(t=0)}{e\left[\tau\left(1 - \frac{1}{n_0}\left\langle \int d^3v F_0 J_0 e^{-iQ}\overline{J_0 e^{iQ}} \right\rangle\right) + 1 - \frac{1}{n_0}\left\langle \int d^3v F_{0e} J_{0e} e^{-iQ_e}\overline{J_{0e} e^{iQ_e}} \right\rangle\right]}. \tag{30}$$

Notice in the *R-H* zonal flow model, the perturbed density remains constant. Therefore, the zonal flow residual is then given by

$$\frac{\phi_k(t=\infty)}{\phi_k(t=0)} = \frac{\tau\left(1 - \frac{1}{n_0}\left\langle \int d^3v F_0 J_0^2 \right\rangle\right) + 1 - \frac{1}{n_0}\left\langle \int d^3v F_{0e} J_{0e}^2 \right\rangle}{\tau\left(1 - \frac{1}{n_0}\left\langle \int d^3v F_0 J_0 e^{-iQ}\overline{J_0 e^{iQ}} \right\rangle\right) + 1 - \frac{1}{n_0}\left\langle \int d^3v F_{0e} J_{0e} e^{-iQ_e}\overline{J_{0e} e^{iQ_e}} \right\rangle}. \tag{31}$$

Using the techniques of the preceding section, we can evaluate this expression numerically and plot the zonal flow residual as a function of $k_\perp \rho_i$ for various safety factors $q$ and inverse aspect ratios $\varepsilon$, as shown in Fig. 4. When the radial wavelength is much smaller than one ion gyroradius and much larger than one electron poloidal gyroradius $\rho_{pe}$, $1 - \frac{1}{n_0}\left\langle \int d^3v F_0 J_0^2 \right\rangle \simeq$

$1-1/\left(\sqrt{2\pi}k_\perp\rho_i\right)$ and $1-\frac{1}{n_0}\left\langle\int d^3vF_0J_0e^{-iQ}\overline{J_0e^{iQ}}\right\rangle\simeq 1$ for ions, and $1-\frac{1}{n_0}\left\langle\int d^3vF_{0e}J_{0e}^2\right\rangle\simeq k_\perp^2\rho_e^2\ll 1$ and $1-\frac{1}{n_0}\left\langle\int d^3vF_{0e}J_{0e}e^{-iQ_e}\overline{J_{0e}e^{iQ_e}}\right\rangle\simeq k_\perp^2\left(\rho_e^2+1.6\varepsilon^{3/2}\rho_{pe}^2\right)\ll 1$ for electrons. In this limit, the result of Eq.(8) of Ref. [12] is recovered. When the ion contribution is close to unity, the electron contribution can be ignored. Therefore, the curves in Fig. 4 show the same behavior as Fig. 3 for $k_\perp\rho_i\lesssim 1$.

When the radial wavelength is comparable to an electron poloidal gyroradius $\rho_{pe}$,

$$\frac{\phi_k\left(t=\infty\right)}{\phi_k\left(t=0\right)}\simeq\tau\frac{1-1/\left(\sqrt{2\pi}k_\perp\rho_i\right)}{1+1.6\varepsilon^{3/2}k_\perp^2\rho_{pe}^2}. \tag{32}$$

The residual increases with $k_\perp\rho_i$ while decreases with $k_\perp\rho_{pe}$. These two tendencies balance when $1/\left(\sqrt{2\pi}k_\perp\rho_i\right)\sim 1.6\varepsilon^{3/2}k_\perp^2\rho_{pe}^2$, making $k_\perp\rho_i\sim\left[\left(\sqrt{\varepsilon}/q^2\right)\left(m_i/m_e\right)\right]^{1/3}$. Hence, when $k_\perp\rho_i<\left[\left(\sqrt{\varepsilon}/q^2\right)\left(m_i/m_e\right)\right]^{1/3}$, the zonal flow residual increases with $k_\perp\rho_i$; but when $k_\perp\rho_i>\left[\left(\sqrt{\varepsilon}/q^2\right)\left(m_i/m_e\right)\right]^{1/3}$, the zonal flow residual decreases with $k_\perp\rho_i$. This trend is shown in Fig. 4.

When $k_\perp\rho_{pe}$ approaches unity, the zonal flow residual can be written as

$$\frac{\phi_k\left(t=\infty\right)}{\phi_k\left(t=0\right)}\simeq\frac{1-1/\left(\sqrt{2\pi}k_\perp\rho_i\right)}{1+k_\perp^2\rho_{pe}^2\left(1.6\varepsilon^{3/2}-\frac{5}{3}\varepsilon^2k_\perp^2\rho_{pe}^2\right)}, \tag{33}$$

where the finite electron poloidal radius effect in Eq.(14) has been retained. Notice that when $\varepsilon^{5/2}k_\perp^2\rho_{pe}^2\sim\varepsilon^{3/2}$, $k_\perp\rho_i\sim\left(\varepsilon^{1/2}/q\right)\sqrt{m_i/m_e}$ and the zonal flow residual begins to increase with $k_\perp\rho_i$, as shown in Fig. 4.

When the radial wavelength is shorter than one electron gyroradius, the initial and final zonal flow potential cannot be affected by either electron or ion polarization. Indeed, the only shielding available for these extremely short wavelengths is *Debye* shielding. Therefore, the zonal flow residual approaches unity as $k_\perp\rightarrow\infty$ . The preceding analysis is sketched in Fig. 5 and is completely consistent with what Jenko *et al.* observed [9].

Of course, the results are sensitive to the form of the initial perturbation. If the initial density perturbation $\delta n_k\left(t=0\right)$ doesn't depend on radial wavelength, $\phi_k\left(t=0\right)\propto\delta n_k\left(t=0\right)/\left(k_\perp^2\rho_i^2\right)$ for $k_\perp^2\rho_i^2\ll 1$ according to Eq.(29), and the residual zonal flow increase in Fig. VII is dramatically altered by this strong source effect for ITG turbulence. However, for the ETG turbulence, $\phi_k\left(t=0\right)\propto\delta n_k\left(t=0\right)$ according to Eq.(29), and there is no strong dependence on the radial wavenumber. Clearly it is desirable to know more detailed information of the initial turbulent perturbation, e.g., the radial wavelength spectrum of $\delta n_k\left(t=0\right)$, to acquire a complete knowledge of the residual zonal flow level.

## VI. SUMMARY AND DISCUSSION

We have extended the collisionless *Rosenbluth-Hinton* residual zonal flow calculation to arbitrary radial wavelengths to retain all finite gyroradius and poloidal gyroradius effects. These effects enter at shorter radial wavelengths tend to increase the residual zonal flow level, but in a non-monotonic fashion as shown in Figs. 4 and 5.

When the radial wavelengths are much larger than electron poloidal gyroradius, only ion polarization is important. The increase in residual flow level from its long wavelength *Rosenbluth-Hinton* value towards a larger value due to finite poloidal gyroradius effects depends on $k_\perp \rho_p$, inverse aspect ratio, and safety factor for the large aspect ratio circular flux surface model considered. An analytic expression valid for $k_\perp \rho_p \lesssim 0.7$ is given. Larger $k_\perp \rho_p$ effects are found by numerically evaluating the integrals in the neoclassical polarization. If finite ion *Larmor* radius effects are neglected by taking $q/\varepsilon \gg 1$, then the transition of the residual to its undamped level ocurs for $\left(k_\perp \rho_p\right)^2 q^2 \sqrt{\varepsilon} \sim 1$. When finite ion gyration effects are retained the residual zonal flow level for even smaller radial wavelengths approaches unity so the initial zonal flow is undamped, with this transition occurring for $k_\perp \rho_i \sim 1$.

When the radial wavelengths are small compared to an ion gyroradius, but comparable to or less than a poloidal electron gyroradius, electron polarization becomes important. The zonal flow residual first decreases with $k_\perp \rho_i$ due to electron neoclassical polarization. Then the zonal flow residual recovers and increases due to the finite electron gyroradius. When the radial wavelengths become less than an electron gyroradius, the zonal flow residual will ultimately approach unity.

## VII. ACKNOWLEDGEMENT

The authors are grateful to Dr. R.E. Waltz for his many helpful comments, insights emails, and notes. The authors also thank Dr. D. Ernst and W. Dorland for many useful discussions and suggestions.

This work was supported by U.S. Department of Energy Grant No. DE-FG02-91ER-54109 at the Massachusetts Institute of Technology.

## REFERENCES


[1] M. Beer, Ph.D. dissertation (1995).

[2] J. Candy and R. Waltz., Phys. Rev. Lett. **91**, 045001 (2003).

[3] D. Ernst et al., Phys. Plasmas **11**, 2637 (2004).

[4] W. Dorland, F. Jenko, M. Kotschenruther, and B. Rogers, Phys. Rev. Lett. **85**, 5579 (2000).

[5] W. Dorland and G. Hammett, Phys. Fluids B **5**, 812 (1993).

[6] G. Hammett, M. Beer, W. Dorland, S. Cowley, and S. Smith, Plasma Phys. Control. Fusion **35**, 973 (1993).

[7] A. Dimits et al., Phys. Plasmas **7**, 969 (2000).

[8] D. Ernst et al., Proc. 20th Int'l. Atomic Energy Agency Fusion Energy Conference(Vilamoura, Portugal 2004), oral paper IAEA-CN-116/TH/4-1. http://www-naweb.iaea.org/napc/physics/fec/fec2004/datasets/TH_4-1.html.

[9] F. Jenko, W. Dorland, M. Kotschenreuther, and B. Rogers, Phys. Plasma **7**, 1904 (2000).

[10] M. Rosenbluth and F. Hinton, Phys. Rev. Lett. **80**, 724 (1998).

[11] F. Hinton and M. Rosenbluth, Plasma Phys. Control. Fusion **41**, A653 (1999).

[12] E. Kim, C. Holland, and P. Diamond, Phys. Rev. Lett. **91**, 075003 (2003).

[13] R. Waltz, Private Communication (2006).

[14] Z. Lin, T. Hahm, W. Lee, W. Tang, and R. White, Science **281**, 1835 (1998).

[15] G. McKee et al., Phys. Plasmas **10**, 1712 (2003).

[16] T. Rhodes, J.-N. Leboeuf, R. Sydora, et al., Phys. Plasmas **9**, 2141 (2002).

[17] P. Helander and D. Sigmar, *Collisional Transport in Magnetized Plasmas*, Wiley, New York, 2001.

[18] S. Zheng, A. Wootton, and E. Solano, Phys. Plasmas **3**, 1176 (1996).

[19] Y. Xiao and P. Catto, to appear in Phys. Plasmas (2006).

**FIGURE CAPTIONS**

Fig. 1 The neoclassical polarization $\varepsilon^{pol}_{k,nc}$ in units of $\frac{\omega^2_{pi}/\omega^2_{ci}}{k^2_\perp \rho^2_i}$, as a function of the inverse aspect ratio $\varepsilon$ for various perpendicular wavenumbers $k_\perp \rho_p$. The solid curves represent the analytical results from Eq.(13), and the discrete shapes represent the numerical results.

Fig. 2 The residual zonal flow potential for a constant initial potential varies with the perpendicular wavelength $k_\perp \rho_i$ for $\varepsilon = 0.1$ and 0.2, according to the analytic formula.

Fig. 3 The residual zonal flow potential for a unit initial potential varies with the radial wavelength $k_\perp \rho_i$. Only ion polarization effect is included.

Fig. 4 The residual zonal flow potential for a unit initial potential varies with the normalized radial wavelength $k_\perp \rho_i$ for $\tau = 1$. Both ion and electron polarization effects are included.

Fig. 5 A schematic plot of zonal flow residual varying with radial wavelength.

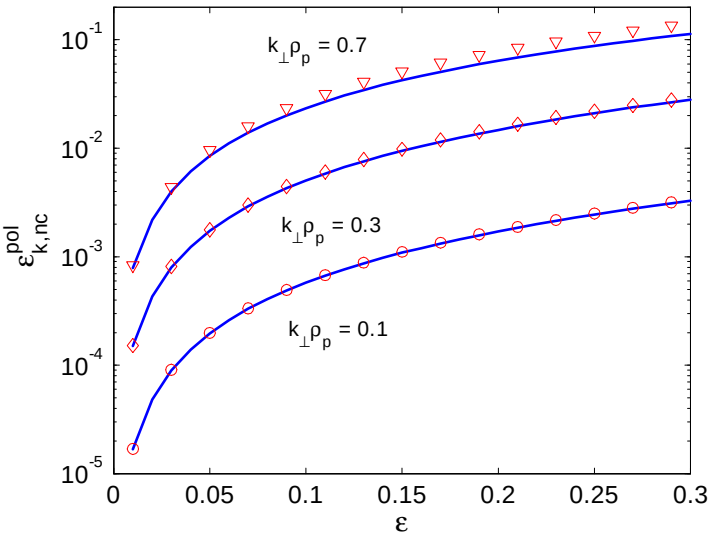


**Figure 1**

**Y. Xiao, P.J. Catto**

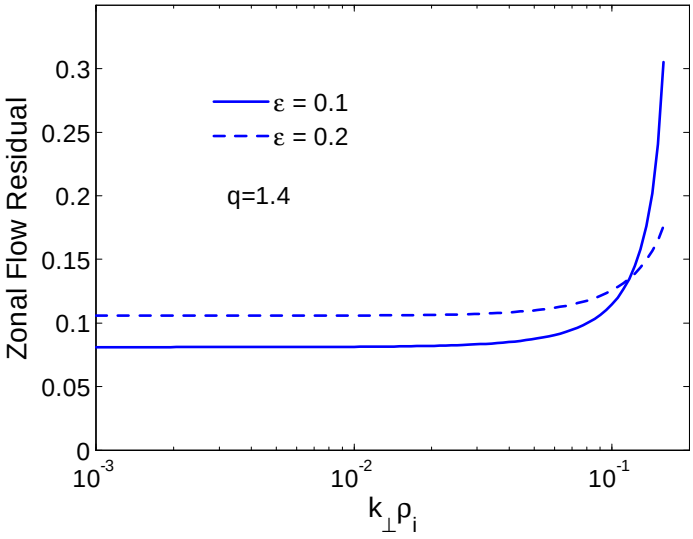


**Figure 2**

**Y. Xiao, P.J. Catto**

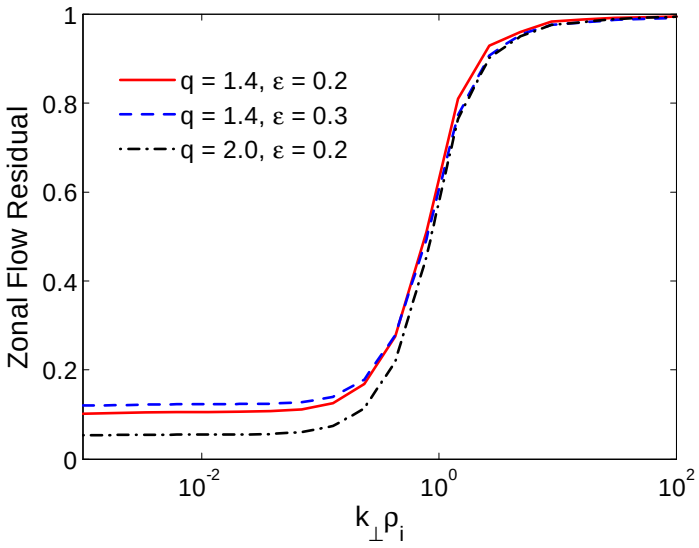


**Figure 3**

**Y. Xiao, P.J. Catto**

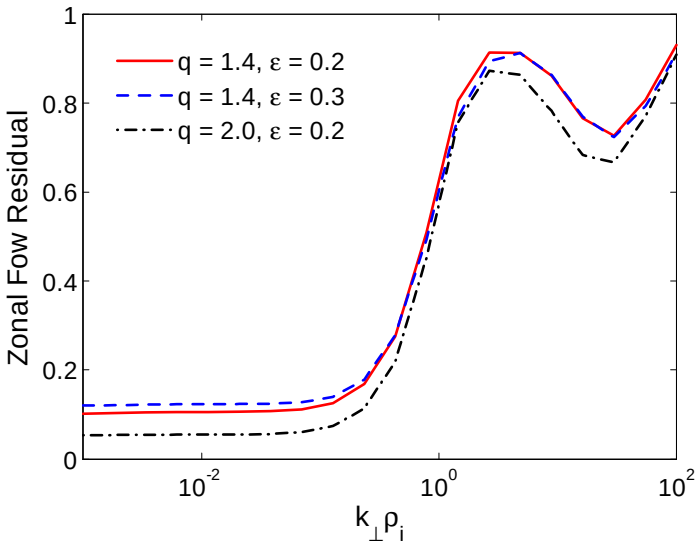


**Figure 4**

**Y. Xiao, P.J. Catto**

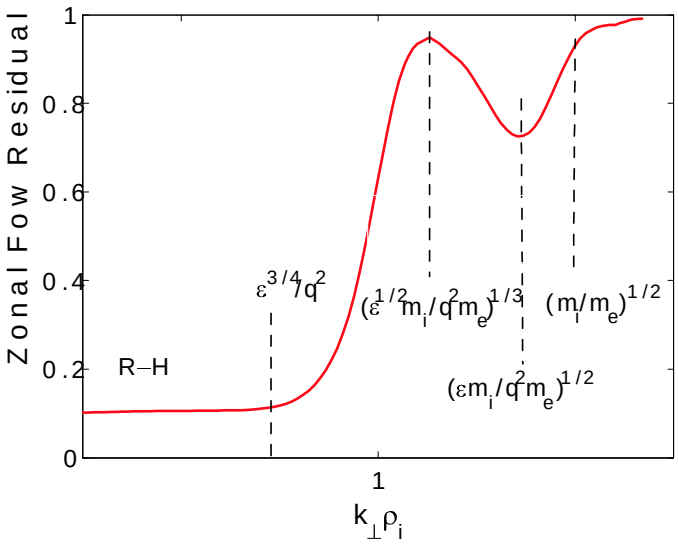


**Figure 5**

**Y. Xiao, P.J. Catto**

## APPENDIX A: DETAILS ABOUT LARGE $Q$ CALCULATION

This appendix presents algebraic details used to evaluate the collisionless neoclassical polarization to $\mathcal{O}(Q^4)$. In particular, we evaluate the following integrals:

$$\begin{aligned}
&\frac{2\pi}{\oint d\theta h}\int d\lambda \oint \frac{d\theta}{\xi}\overline{Q^2},\ \frac{2\pi}{\oint d\theta h}\int d\lambda \oint \frac{d\theta}{\xi}\overline{Q^4},\\
&\frac{2\pi}{\oint d\theta h}\int_0^{1-\varepsilon} d\lambda \oint \frac{d\theta}{\xi}\overline{Q}^2,\ \frac{2\pi}{\oint d\theta h}\int_0^{1-\varepsilon} d\lambda \oint \frac{d\theta}{\xi}\overline{Q}\ \overline{Q^3},\\
&\frac{2\pi}{\oint d\theta h}\int d\lambda \oint \frac{d\theta}{\xi}\overline{Q^2}^2,
\end{aligned} \tag{A1}$$

with $h = B_0/B = 1 + \varepsilon\cos\theta$, $B_0$ is the magnetic field at the magnetic axis. The integration is carried out based on a large aspect ratio circular tokamak model, namely the arc length $dl = qR_0 d\theta$ and the magnetic field $B_0/B = 1 + \varepsilon\cos\theta$.

The first two integrals can be carried out by using the following identities:

$$\int d^3v v_\parallel^2 F_0 = n_0\frac{T_i}{m_i}, \tag{A2}$$

$$\int d^3v v_\parallel^4 F_0 = 3n_0\left(\frac{T_i}{m_i}\right)^2. \tag{A3}$$

We first note that we can use the preceding identities to obtain

$$\begin{aligned}
\left\langle \int d^3v F_0 \overline{Q^2}\right\rangle &= \left(\frac{IS'}{\Omega_0}\right)^2\left\langle h^2\int d^3v v_\parallel^2 F_0\right\rangle\\
&= n_0\frac{T_i}{m_i}\left(\frac{IS'}{\Omega_0}\right)^2\left(1+\frac{3}{2}\varepsilon^2\right),
\end{aligned} \tag{A4}$$

and

$$\begin{aligned}
\left\langle \int d^3v F_0 \overline{Q^4}\right\rangle &= \left(\frac{IS'}{\Omega_0}\right)^4\left\langle h^4\int d^3v v_\parallel^4 F_0\right\rangle\\
&= 3n_0\left(\frac{T_i}{m_i}\right)^2\left(\frac{IS'}{\Omega_0}\right)^4\left(1+5\varepsilon^2+\frac{15}{8}\varepsilon^4\right).
\end{aligned} \tag{A5}$$

Alternatively, we can write these two integrals as

$$\left\langle \int d^3v F_0 \overline{Q^2}\right\rangle = \frac{3n_0T_i}{4\pi m_i}\left(\frac{IS'}{\Omega_0}\right)^2\int d\lambda\oint\frac{d\theta}{\xi}(\xi h)^2 \tag{A6}$$

and

$$\left\langle \int d^3v F_0 \overline{Q^4}\right\rangle = \frac{15n_0}{4\pi}\left(\frac{T_i}{m_i}\right)^2\left(\frac{IS'}{\Omega_0}\right)^4\int d\lambda\oint\frac{d\theta}{\xi}(\xi h)^4. \tag{A7}$$

Comparing the preceding four equations, we obtain

$$\frac{2\pi}{\oint d\theta h}\int d\lambda \oint \frac{d\theta}{\xi}\left(\xi h\right)^2 = \frac{4\pi}{3}\left(1+\frac{3}{2}\varepsilon^2\right) \tag{A8}$$

and

$$\frac{2\pi}{\oint d\theta h}\int d\lambda \oint \frac{d\theta}{\xi}\left(\xi h\right)^4 = \frac{4\pi}{5}\left(1+5\varepsilon^2+\frac{15}{8}\varepsilon^4\right). \tag{A9}$$

Therefore,

$$\frac{2\pi}{\oint d\theta h}\int d\lambda \oint \frac{d\theta}{\xi}\overline{Q^2} = \frac{8\pi}{3}\left(1+\frac{3}{2}\varepsilon^2\right)\frac{m_i E}{T_i}\left(k_\perp \rho_p\right)^2, \tag{A10}$$

and

$$\frac{2\pi}{\oint d\theta h}\int d\lambda \oint \frac{d\theta}{\xi}\overline{Q^4} = \frac{16\pi}{5}\left(1+5\varepsilon^2+\frac{15}{8}\varepsilon^4\right)\left(\frac{m_i E}{T_i}\right)^2\left(k_\perp \rho_p\right)^4 \tag{A11}$$

with $k_\perp \rho_p = \frac{IS'}{\Omega_0}\sqrt{\frac{T_i}{m_i}}$, and $E = v^2/2$.

The third and fourth integrals in Eq.(A1) involve only passing particles. The usual way to deal with them utilizes *elliptic integrals*. Here we employ an alternate method based on an $\varepsilon$ expansion to carry out the integrations.

First, we consider the integral $\int_0^{1-\varepsilon} d\lambda \oint \frac{d\theta}{\xi}\overline{Q}^2$, where

$$\frac{2\pi}{\oint d\theta h}\oint \frac{d\theta}{\xi}\overline{Q}^2 = \left(k_\perp \rho_p\right)^2 \frac{4\pi m_i E}{T_i}\frac{2\pi}{\oint \frac{d\theta}{\xi}}. \tag{A12}$$

For a large aspect ratio circular tokamak we have

$$\frac{1}{\xi} = \sqrt{\frac{1+\varepsilon\cos\theta}{1-\lambda+\varepsilon\cos\theta}}. \tag{A13}$$

If we let $x = 1-\lambda$, then $\varepsilon < x < 1$ for passing particles. We may then expand $1/\xi$ to order $\varepsilon^M$,

$$\begin{aligned}\frac{1}{\xi} = \frac{1}{\sqrt{x}}[1 &+ \frac{1}{2}\left(1-\frac{1}{x}\right)\varepsilon\cos\theta + \\ &+ \left(-\frac{1}{8}-\frac{1}{4x}+\frac{3}{8x^2}\right)\varepsilon^2\cos^2\theta + .. + O\left(\varepsilon^{M+1}\right)],\end{aligned} \tag{A14}$$

where the expansion order $M$ depends on the accuracy desired for the integral $\int_0^{1-\varepsilon} d\lambda \oint \frac{d\theta}{\xi}\overline{Q}^2$. Therefore,

$$\oint \frac{d\theta}{\xi} = \frac{1}{\sqrt{x}}\sum_{n=0}^{M} a_n\left(\frac{1}{x}\right)\varepsilon^n, \tag{A15}$$

where the coefficient $a_n\left(\frac{1}{x}\right)$ is an $n$th order polynomial in $1/x$, with $a_0\left(\frac{1}{x}\right) = 2\pi$, and

$$a_2\left(\frac{1}{x}\right) = 2\pi\left(\frac{3}{16x^2}-\frac{1}{8x}-\frac{1}{16}\right), \tag{A16}$$

for $M=2$, for example. In fact, only even $n$ terms survive the $\theta$ integration since $a_{2m+1}\left(\frac{1}{x}\right)=0$, for $m=0,1,2....$ Using Eq.(A15) we find

$$\frac{2\pi}{\oint\frac{d\theta}{\xi}}=\sqrt{x}\sum_{n=0}^{M}b_n\left(\frac{1}{x}\right)\varepsilon^n, \tag{A17}$$

where $b_0=1$,

$$b_2=-\frac{3}{16x^2}+\frac{1}{8x}+\frac{1}{16}, \tag{A18}$$

and $b_{2m+1}\left(\frac{1}{x}\right)=0$, for $m=0,1,2....$ Using Eqs.(A17) and (A12) for $M=2$ we find, for example, that

$$\begin{aligned}\int_0^{1-\varepsilon}d\lambda\oint\frac{d\theta}{\xi}\overline{Q}^2&=\int_\varepsilon^1 dx\oint\frac{d\theta}{\xi}\overline{Q}^2\\&=\left(k_\perp\rho_p\right)^2\frac{4\pi m_iE}{T_i}\left(\frac{2}{3}-\frac{25}{24}\varepsilon^{3/2}+\frac{2}{3}\varepsilon^2\right).\end{aligned} \tag{A19}$$

We next increase the expansion order $M$ to obtain a more precise result. The coefficient polynomial $b_n\left(\frac{1}{x}\right)$ has the following form

$$b_n\left(\frac{1}{x}\right)=\sum_{k=0}^{n}b_n^{(k)}/x^k, \tag{A20}$$

where the numerical coefficients $b_n^{(k)}$ in the preceding $M=2$ case can be evaluated using the preceding expansion procedure, e.g.,

$$b_2^{(2)}=-\frac{3}{16},\ b_2^{(1)}=\frac{1}{8},\ b_2^{(0)}=\frac{1}{16}. \tag{A21}$$

Once all the numerical coefficients in Eq.(A20) are determined from Eq.(A14) we obtain

$$\begin{aligned}\int_0^{1-\varepsilon}d\lambda\oint\frac{d\theta}{\xi}\overline{Q}^2&=\left(k_\perp\rho_p\right)^2\frac{4\pi m_iE}{T_i}\int_\varepsilon^1 dx\sqrt{x}\sum_{m=0}^{M/2}b_{2m}\left(\frac{1}{x}\right)\varepsilon^{2m}\\&=\left(k_\perp\rho_p\right)^2\frac{4\pi m_iE}{T_i}\sum_{m=0}^{M/2}\varepsilon^{2m}\sum_{k=0}^{2m}b_{2m}^{(k)}\int_\varepsilon^1 dx\frac{\sqrt{x}}{x^k}.\end{aligned} \tag{A22}$$

The preceding integrals can be easily carried out to obtain

$$\int_0^{1-\varepsilon}d\lambda\oint\frac{d\theta}{\xi}\overline{Q}^2=\left(k_\perp\rho_p\right)^2\frac{4\pi m_iE}{T_i}\sum_{m=0}^{M/2}\varepsilon^{2m}\sum_{k=0}^{2m}\frac{b_{2m}^{(k)}}{3/2-k}\left(1-\varepsilon^{3/2-k}\right). \tag{A23}$$

If we write

$$\sum_{m=0}^{M/2}\varepsilon^{2m}\sum_{k=0}^{2m}\frac{b_{2m}^{(k)}}{3/2-k}\left(1-\varepsilon^{3/2-k}\right)=\sum_{k=0}^{2M}\Upsilon_{k/2}\varepsilon^{k/2}, \tag{A24}$$

then

$$\Upsilon_0 = \frac{b_0^{(0)}}{3/2} \to \frac{2}{3}, \tag{A25}$$

and $\Upsilon_{1/2} = \Upsilon_1 = 0$, and

$$\Upsilon_{3/2} = -\sum_{m=0}^{2M} b_{2m}^{(2m)} \frac{1}{3/2 - 2m}. \tag{A26}$$

Although the preceding expression is an infinite series, we find this series converges very rapidly. Just keeping the first several terms we obtain the following precise result

$$\Upsilon_{3/2} \to -1.09. \tag{A27}$$

Following this procedure, we can also easily obtain

$$\Upsilon_2 = \frac{b_2^{(0)}}{3/2} + \frac{b_2^{(1)}}{3/2 - 1} + \frac{b_2^{(2)}}{3/2 - 2} \to \frac{2}{3}. \tag{A28}$$

Therefore, to order $\mathcal{O}(\varepsilon^2)$ we find

$$\sum_{m=0}^{M/2} \varepsilon^{2m} \sum_{k=0}^{2m} \frac{b_{2m}^{(k)}}{3/2 - k} \left(1 - \varepsilon^{3/2-k}\right) \to \frac{2}{3} - 1.09\varepsilon^{3/2} + \frac{2}{3}\varepsilon^2.$$

In general, the integer power coefficients $\Upsilon_n$ in Eq.(A24) only depend on the coefficients $b_n^{(k)}$, $k = 0, 1, 2, ..., n$, or the polynomial $b_n\left(\frac{1}{x}\right)$. However, the half integer power coefficients $\Upsilon_{(2n+1)/2}$ in Eq.(A24) require an infinite series to approach the exact value. Fortunately, this series converges very rapidly. The expansion procedure we described here is different from the conventional approach that uses *elliptic integral*s. We expand the integrand from the beginning to avoid the *elliptic integral*s since we know the final result will be a *Taylor* series in inverse aspect ratio $\varepsilon$. This approach is algebraically less involved and makes some complicated integrals easier to handle. Using this expansion procedure, we obtain

$$\frac{2\pi}{\oint d\theta h} \int_0^{1-\varepsilon} d\lambda \oint \frac{d\theta}{\xi} \overline{Q}^2 = (k_\perp \rho_p)^2 \frac{m_i E}{T_i} \frac{8\pi}{3} (1 - 1.635\varepsilon^{3/2} + \varepsilon^2 - 0.36\varepsilon^{5/2} - 0.0285\varepsilon^{7/2}), \tag{A29}$$

which is accurate to $\mathcal{O}(\varepsilon^4)$.

Next we evaluate the integral $\frac{2\pi}{\oint d\theta h} \int_0^{1-\varepsilon} d\lambda \oint \frac{d\theta}{\xi} \overline{Q}\ \overline{Q^3}$ in Eq.(A1):

$$\frac{2\pi}{\oint d\theta h} \int_0^{1-\varepsilon} d\lambda \oint \frac{d\theta}{\xi} \overline{Q}\ \overline{Q^3} = (k_\perp \rho_p)^4 \left(\frac{2m_i E}{T_i}\right)^2 \frac{\oint d\theta h \oint d\theta \xi^2 h^3}{\oint \frac{d\theta}{\xi}}, \tag{A30}$$

where

$$\oint d\theta\xi^2 h^3 = \oint d\theta\,(1-\lambda/h)\,h^3$$
$$= 2\pi\left(1+\frac{3}{2}\varepsilon^2-\lambda\left(1+\frac{1}{2}\varepsilon^2\right)\right). \tag{A31}$$

Therefore,

$$\frac{2\pi}{\oint d\theta h}\oint\frac{d\theta}{\xi}\overline{Q}\;\overline{Q^3} = (k_\perp\rho_p)^4\left(\frac{2m_iE}{T_i}\right)^2\frac{2\pi}{\oint\frac{d\theta}{\xi}}(1+\frac{3}{2}\varepsilon^2$$
$$-\lambda\left(1+\frac{1}{2}\varepsilon^2\right)). \tag{A32}$$

We can apply the same technique as we did to evaluate $\int_0^{1-\varepsilon}d\lambda\oint\frac{d\theta}{\xi}\overline{Q}^2$ to obtain

$$\frac{2\pi}{\oint d\theta h}\int_0^{1-\varepsilon}d\lambda\oint\frac{d\theta}{\xi}\overline{Q}\;\overline{Q^3} = (k_\perp\rho_p)^4\left(\frac{m_iE}{T_i}\right)^2\frac{16\pi}{5}(1+\frac{3}{2}\varepsilon^2 \tag{A33}$$
$$-0.23\varepsilon^{5/2}-2.86\varepsilon^{7/2}). \tag{A34}$$

The final integral in Eq.(A1), $\frac{2\pi}{\oint d\theta h}\int d\lambda\oint\frac{d\theta}{\xi}\overline{Q^2}^2$, contains both passing and trapped particle contributions. For the passing particle contribution we follow the same procedure as we did to evaluate $\frac{2\pi}{\oint d\theta h}\int_0^{1-\varepsilon}d\lambda\oint\frac{d\theta}{\xi}\overline{Q}^2$ to obtain

$$\frac{2\pi}{\oint d\theta h}\int_0^{1-\varepsilon}d\lambda\oint\frac{d\theta}{\xi}\overline{Q^2}^2 = (k_\perp\rho_p)^4\left(\frac{2m_iE}{T_i}\right)^2\int_0^{1-\varepsilon}d\lambda\frac{\left(\oint d\theta\xi h^2\right)^2}{\oint\frac{d\theta}{\xi}}$$
$$= (k_\perp\rho_p)^4\left(\frac{2m_iE}{T_i}\right)^2(\frac{4\pi}{5}+\frac{4\pi}{15}\varepsilon^2$$
$$+1.0\varepsilon^{5/2}-5.4\varepsilon^{7/2}+\frac{7\pi}{5}\varepsilon^4). \tag{A35}$$

The trapped particle contribution is more complicated and may be written as

$$\frac{2\pi}{\oint d\theta h}\int_{1-\varepsilon}^{1+\varepsilon}d\lambda\oint\frac{d\theta}{\xi}\overline{Q^2}^2 = (k_\perp\rho_p)^4\left(\frac{2m_iE}{T_i}\right)^2\int_{1-\varepsilon}^{1+\varepsilon}d\lambda\frac{\left(\oint d\theta\xi h^2\right)^2}{\oint\frac{d\theta}{\xi}}, \tag{A36}$$

where we need to evaluate both $\oint d\theta\xi h^2$ and $\oint\frac{d\theta}{\xi}$ for the trapped particles. First, we have

$$\oint d\theta\xi h^2 = 2\int_0^{\theta_b}d\theta\sqrt{1-\lambda+\varepsilon\cos\theta}\,(1+\varepsilon\cos\theta)^{3/2}, \tag{A37}$$

where the turning angle $\theta_b$ is defined by $\theta_b=\arccos\left(\frac{1-\lambda}{\varepsilon}\right)$. We may define $\tau\equiv\frac{1-\lambda+\varepsilon}{2\varepsilon}=\sin^2(\theta_b/2)$, and $\sin\eta\equiv\sin(\theta/2)/\sin(\theta_b/2)$, then

$$d\theta=\frac{2\sin\frac{\theta_b}{2}\cos\eta}{\sqrt{1-\tau\sin^2\eta}}d\eta. \tag{A38}$$

Hence, Eq.(A37) can be evaluated as

$$\begin{aligned}\oint d\theta \xi h^2 &\cong 2\sqrt{2\varepsilon}\int_0^{\theta_b} d\theta \sqrt{\tau-\sin^2\frac{\theta}{2}}\left(1+\frac{3}{2}\varepsilon\cos\theta\right)\\ &= 4\sqrt{2\varepsilon}\tau\int_0^{\pi/2} d\eta \frac{1-\sin^2\eta}{\sqrt{1-\tau\sin^2\eta}}\left[1+\frac{3}{2}\varepsilon\left(1-2\tau\sin^2\eta\right)\right]\\ &= 2\sqrt{2\varepsilon}\left\{\left[2+\varepsilon\left(2\tau-1\right)\right]E\left(\tau\right)+\left(\tau-1\right)\left(2-\varepsilon\right)K\left(\tau\right)\right\},\end{aligned} \tag{A39}$$

where $K(\tau)$ and $E(\tau)$ are complete *Elliptic Integrals* of the first and second kind, respectively. Similarly, we obtain the bounce time for the trapped particles

$$\oint \frac{d\theta}{\xi} = \frac{4}{\sqrt{2\varepsilon}}\left[\left(1-\frac{1}{2}\varepsilon\right)K\left(\tau\right)+\varepsilon E\left(\tau\right)\right]. \tag{A40}$$

Using the preceding two equations, the integral in Eq.(A35) can be written as

$$\begin{aligned}\int_0^{1-\varepsilon} d\lambda \oint \frac{d\theta}{\xi}\overline{Q^2}^2 = \left(k_\perp\rho_p\right)^4\left(\frac{2m_iE}{T_i}\right)^2\left(2\varepsilon\right)^{3/2}\int_0^1 d\tau\\ \frac{\left\{\left[2+\varepsilon\left(2\tau-1\right)\right]E\left(\tau\right)+\left(\tau-1\right)\left(2-\varepsilon\right)K\left(\tau\right)\right\}^2}{\left(1-\frac{1}{2}\varepsilon\right)K\left(\tau\right)+\varepsilon E\left(\tau\right)}.\end{aligned} \tag{A41}$$

This integral can be expanded in $\varepsilon$ and then evaluated numerically to obtain

$$\frac{2\pi}{\oint d\theta h}\int_0^{1-\varepsilon} d\lambda \oint \frac{d\theta}{\xi}\overline{Q^2}^2 = \left(k_\perp\rho_p\right)^4\left(\frac{2m_iE}{T_i}\right)^2\left[2.68\varepsilon^{5/2}+4.4\varepsilon^{7/2}+\mathcal{O}\left(\varepsilon^{9/2}\right)\right]. \tag{A42}$$

From this expression we see that the trapped particle contribution only contains half integer powers of $\varepsilon$.

Terms of $\mathcal{O}(\varepsilon^2)$ are ignored in the preceding large aspect ratio circular tokamak model. For a more realistic circular tokamak, higher order terms proportional to $\varepsilon^2$ need to be kept to make the preceding $\varepsilon$ expansions accurate to order $\varepsilon^2$. For a global equilibrium satisfying *Grad-Shafranov* equation with the drives $dp/d\psi$ and $IdI/d\psi$ constant [17][18][19], we may assume the elongation to be unity, the triangularity and *Shafranov* shift to be zero, and only keep the safety factor $q$ as a parameter along with $\varepsilon$. In such a circular tokamak model, the arc length is $dl = qR_0\left[1+\left(\frac{1}{2q^2}-\frac{1}{2}\right)\varepsilon^2\right]d\theta$ and the magnetic field $B_0/B = 1+\varepsilon\cos\theta-\varepsilon^2/\left(2q^2\right)$. Following the previous procedure, we find

$$\frac{2\pi}{\oint d\theta h}\int d\lambda \oint \frac{d\theta}{\xi}\left(\xi h\right)^2 = \frac{m_iE}{T_i}\left(k_\perp\rho_p\right)^2\frac{8\pi}{3}\left[1+\left(\frac{3}{2}-\frac{1}{q^2}\right)\varepsilon^2+\mathcal{O}\left(\varepsilon^4\right)\right], \tag{A43}$$

and

$$\frac{2\pi}{\oint d\theta h}\int d\lambda \oint \frac{d\theta}{\xi}\overline{Q^4} = \left(\frac{m_iE}{T_i}\right)^2\left(k_\perp\rho_p\right)^4\frac{16\pi}{5}\left[1+\left(5-\frac{2}{q^2}\right)\varepsilon^2+\mathcal{O}\left(\varepsilon^4\right)\right], \tag{A44}$$

and

$$\frac{2\pi}{\oint d\theta h}\int_0^{1-\varepsilon} d\lambda \oint \frac{d\theta}{\xi}\overline{Q}^2 = \frac{m_i E}{T_i}\left(k_\perp \rho_p\right)^2 \frac{8\pi}{3}[1 - 1.63\varepsilon^{3/2} + (1 - \frac{1}{q^2})\varepsilon^2 - 0.36\varepsilon^{5/2} + (\frac{0.41}{q^2} - 0.03)\varepsilon^{7/2}], \tag{A45}$$

and

$$\frac{2\pi}{\oint d\theta h}\int_0^{1-\varepsilon} d\lambda \oint \frac{d\theta}{\xi}\overline{Q}\ \overline{Q^3} = \left(\frac{m_i E}{T_i}\right)^2 \left(k_\perp \rho_p\right)^4 \frac{16\pi}{5}[1 + (\frac{3}{2} - \frac{2}{q^2})\varepsilon^2 - 0.23\varepsilon^{5/2} - 2.86\varepsilon^{7/2}], \tag{A46}$$

and

$$\frac{2\pi}{\oint d\theta h}\int d\lambda \oint \frac{d\theta}{\xi}\overline{Q^2}^2 = \left(\frac{m_i E}{T_i}\right)^2 \left(k_\perp \rho_p\right)^4 [\frac{4\pi}{5} + (\frac{4\pi}{15} - \frac{8\pi}{5q^2})\varepsilon^2 + \varepsilon^{5/2} - 5.38\varepsilon^{7/2}]. \tag{A47}$$

We see that the explicit $q$ factors in the Eq.(12) cancel out, leaving the result in Eq.(14) that only contains $q$ factors implicitly through $k_\perp^2 \rho_p^2$. Although this result is expanded to $\varepsilon^{7/2}$ for completeness, it is actually only accurate to $\varepsilon^{5/2}$ because the MHD equilibrium we use is only accurate to order $\varepsilon^2$.